Tandem Mass Spectrometry of Protein–Protein Complexes: Cytochrome *c*–Cytochrome b_5

M. R. Mauk and A. G. Mauk
Department of Biochemistry and Molecular Biology, University of British Columbia, Vancouver, British Columbia, Canada

Yu-Luan Chen[†] and D. J. Douglas*
Department of Chemistry, University of British Columbia, Vancouver, British Columbia, Canada

An improved method to interpret triple quadrupole MS/MS experiments of complexes of large ions is presented and applied to a study of the complex formed by the proteins cytochrome *c* and cytochrome b_5. Modeling of the activation and dissociation process shows that most of the reaction occurs near the collision cell exit where ions have the highest internal energies. Experiments at different collision cell pressures or with different collision gases (Ne, Ar, Kr) are interpreted with a previously proposed collision model (Chen et al., *Rapid Commun. Mass Spectrom.* **1998,** *12*, 1003–1010) to calculate the internal energy added to ions to cause dissociation. Small but systematic differences under different experimental conditions are attributed to different times available for reaction. A method to correct for this is presented. Ne, Ar, and Kr are found to have similar energy transfer efficiencies. Complexes of cytochrome *c* and cytochrome b_5 are detected in ESI mass spectra but with abundances less than expected from the solution equilibrium. Dissociation of the cytochrome *c*–cytochrome b_5 complexes with charge k gives as the most abundant fragments, cytochrome b_5^{+3} and cytochrome $c^{+(k-3)}$. Adding charges to the complex destabilizes it. A series of cytochrome *c* variants with Lys residues thought to be involved in solution binding replaced by Ala showed no differences in the energy required to induce dissociation of the gas phase complex. The implications for the binding of the gas phase ions are inconclusive. (J Am Soc Mass Spectrom 2002, 13, 59–71) © 2002 American Society for Mass Spectrometry

Electrospray ionization mass spectrometry allows the observation of gas phase ions of intact noncovalent complexes of biomolecules [1]. These complexes are formed in solution through highly specific interactions that allow the species to "recognize" each other. The structures of ions of noncovalent complexes in the gas phase are of special interest. If conditions can be found where the gas phase ions retain the same specific binding that allows the partners to "recognize" each other in solution, mass spectrometry may find widespread application to the measurement of at least relative binding energies. Detailed insights into the gas phase binding can be obtained if a related series of complexes are available which have different binding strengths in solution. For example, with proteins, residues that are involved in solution binding can be altered by site directed mutagenesis or other means to change the solution binding energy. Comparisons between gas phase and solution complexes can then determine if the same residues are involved in gas phase binding.

Gas phase binding can be probed by blackbody infrared radiative dissociation (BIRD) experiments [2], dissociation in the orifice-skimmer region of an ion sampling interface [3], thermal dissociation of ions trapped in a quadrupole field [4], and tandem mass spectrometry with trap [6] or triple quadrupole [7] systems. BIRD and thermal dissociation experiments are attractive because they give rate constants for unimolecular dissociation of complexes, which, if interpreted with transition state theory, provide dissociation barriers and entropies of activation. However these experiments are limited to those complexes which can be dissociated in the somewhat limited temperature range of the experiments.

Tandem mass spectrometry experiments attempt to measure the additional internal energy that must be added to an ion, ΔE_{int}, to induce dissociation (i.e., the energy above that which an ion contains from the source, E^0_{int}. In many experiments E^0_{int} is unknown.) The collision energy is systematically increased, and the point at which the precursor ion intensity is reduced to half (or some other value) is often taken as a measure of the additional energy required to cause dissociation on

Published online November 20, 2001

Address reprint requests to Dr. D. J. Douglas, Department of Chemistry, University of British Columbia, 2036 Main Mall, Vancouver, BC V6T 1Z1, Canada. E-mail: douglas@chem.ubc.ca

[†]Current address: Covance Laboratories Inc., P.O. Box 7545, Madison, Wisconsin 53707-7545, USA.

1044-0305/02/$20.00
PII S1044-0305(01)00331-2

Received June 12, 2001
Revised September 17, 2001
Accepted September 17, 2001

the time scale of the experiment. This has been described for ICR [5], 3D ion trap [6], and triple quadrupole mass spectrometers [7]. In trap experiments the amplitude or duration of the excitation voltage used to induce dissociation can be varied systematically; in triple quadrupole experiments the energy with which ions are injected into the collision cell is usually varied. These parameters are not related to the dissociation energy in any simple way. Determination of the added internal energy in ICR experiments is particularly complex [8]. In comparison, the motion of an ion passing through the collision cell of a triple quadrupole system is more easily modeled [7b, 9].

Previously, we proposed a model to calculate the energy transferred to large ions, ΔE_{int}, as they pass through the collision cell of a triple quadrupole system [7b]. In this model ions accumulate energy in a series of inelastic collisions. The model corrects for the different numbers of collisions of ions with different cross sections and the kinetic energy losses of ions as they move through the cell. The model was used to assess the binding of heme to highly charged holomyoglobin ions, with the conclusion that high charge states bind heme with energies similar to low charge states even though high charge states are substantially more unfolded.

Cytochrome *c* and cytochrome b_5 are two well characterized proteins with structures, properties, and mutagenesis that have been extensively studied. The noncovalent complex formed by cytochrome *c* and cytochrome b_5 is a model system for studying electron transfer and has been reviewed by Mauk et al. [10]. In solution at pH 7.0, cytochrome *c* is positively charged (average charge +7.31) and cytochrome b_5 is negatively charged (average charge −8.15) [11]. Salemme proposed a model in which binding of the two proteins is mostly derived from formation of salt bridges between positive residues on cytochrome *c* and negative residues on cytochrome b_5 [12]. This model was later refined through a Brownian dynamics simulation of the docking of the proteins [11] and molecular mechanics simulations [13] with the conclusion that salt bridges will most likely form between the positive residues Arg 13, trimethyl lysine (Tml) 72, Lys 86, and Gln 16 residues of cytochrome *c* and the negative residues Glu 48, a heme propionate, Asp 60, and Glu 44 of cytochrome b_5. The association constant for the complex, K_A, decreases with increasing ionic strength (μ) in solution, from $K_A \approx 10^7$ M at $\mu = 0$ to $K_A \approx 10^5$ M at $\mu = 10^{-2}$ M [14]. The association constant also decreases for pH values different from 7.0. The binding constant of cytochrome *c*–cytochrome b_5 is almost nine orders of magnitude lower than that of heme binding to myoglobin. Thus, in comparison to many of the noncovalently bound species that have been studied by ESI-MS, cytochrome *c*–cytochrome b_5 complexes are relatively fragile.

In this paper we further model and give a more detailed analysis of the activation and dissociation of complexes of large ions in triple quadrupole MS/MS systems. The complex formed by the proteins cytochrome *c* and cytochrome b_5 is studied in detail with various collision gases and at various collision gas pressures. A simulation of the activation process shows that most of the dissociation occurs near the exit of the collision cell, where ions have the highest internal energies. It is shown that small but systematic differences in the energy required to induce dissociation, ΔE_{int}, calculated with our earlier model, can be attributed to differences in the time available for dissociation of ions under different experimental conditions. A method to correct for this effect is presented. The results are the most detailed study yet of the activation and dissociation process for large molecule complexes in a triple quadrupole system.

Our initial goal in this work was to study native and mutant cytochromes with different binding energies in solution and to compare trends of dissociation energies between solution and gas phase ions. Collision cross sections show that the complexes have relatively compact structures. MS/MS spectra reveal the fragmentation pathways of the complex ions and the possible charge distribution in the ions. A series of complexes with cytochrome *c* variants, trimethyl-Lys72Ala, Lys73Ala, Lys79Ala, and Lys87Ala with similar binding energies in solution were run and the results interpreted with the improved model described here. These mutations were found to produce no measurable changes to the internal energies required to induce dissociation of the complexes. However it cannot be determined if these residues are involved in the binding of the gas phase complexes.

Collision Models

Kinetic Shifts

It has been noted that for large ions such as peptides, substantial kinetic shifts can be expected [15]. For protein–protein complexes, these effects can be dramatic. Consider a complex with 3000 atoms, molecular weight 23,000 and 9000-6 = 8994 internal degrees of freedom. Suppose the rate constant for dissociation $k(E_{\text{int}})$ is given by the RRK expression

$$k(E_{\text{int}}) = v\left(\frac{E_{\text{int}} - E_0}{E_{\text{int}}}\right)^s \quad (1)$$

where E_{int} is the internal energy, E_0 is the dissociation energy and *s* is the number of degrees of freedom. If appreciable reaction is to occur in 10–100 μs (typical of our triple quadrupole experiments, see below) then the rate constant must be $k(E_{\text{int}}) \approx 10^{-4}\ \text{s}^{-1}$. If, for example, E_0 = 0.5 eV, $v = 10^9$, and s = 8994, then an internal energy of 391 eV is necessary. If the ions begin with thermal energy at 295K, the initial internal energy is 229 eV and so 162 eV must be added to the ion to cause dissociation. Suppose the ion has a collision cross section of 2000 Å^2 and it passes through a 20 cm long

collision cell filled with Ar at a pressure of 1.0 mtorr. The mean free path, λ, is 0.1515 cm, the ion will have 132 collisions, and the ion must acquire 1.22 eV of internal energy per collision. If the collisions are completely inelastic, i.e., if all of the center-of-mass translational energy is converted to internal ion energy in a collision, the center-of-mass energy must be at least 1.22 eV and so the lab energy must be 702 eV. This demonstrates the major differences between dissociation of small molecules and dissociation of large protein complexes in triple quadrupole experiments. Ions of large protein complexes accumulate energy through many collisions and internal energies must be on the order of hundreds of eV.

Collision Model

Earlier, we proposed a model to calculate the internal energy added to large ions, activated in triple quadrupole experiments, which accounts for these features [7b]. The model allows for the fact that ions with different collision cross sections have different numbers of collisions in the cell, and that ions lose kinetic energy as they pass through the collision cell. The internal energy added to an ion, ΔE_{int}, is given by

$$\Delta E_{\text{int}} = \phi \frac{m_2}{M} E^0 \frac{m_1}{m_2} \frac{1}{C_D} \left(1 - \exp - \frac{C_D n m_2 \sigma l}{m_1}\right) \qquad (2)$$

where ϕ is the average efficiency of conversion of center-of-mass energy to internal energy of the ion, m_1 is the ion mass, m_2 is the collision gas mass, $M = m_1 + m_2$, E^0 is the lab translational energy of the ion at the cell entrance, C_D is a drag coefficient [16], n is the number density of the gas in the collision cell, σ is the collision cross section of the ion with the gas, and l is the distance of the ion from the cell entrance. This model assumes a constant collision cross section as the ion passes through the cell. It is possible that as the ion is activated, the increased internal energy can cause the ion to unfold to a conformation with an increased cross section. It is difficult to estimate the effects of this on the ΔE_{int} values. As well it is possible that complexes exist in different conformations with different reactivities. There is no experimental evidence for this in the results described below, but in general this possibility should be considered.

The efficiency of conversion of center-of-mass to internal energy, ϕ, for large protein ions is not known. However there is increasing evidence that ϕ is very high, as follows: (1) A study of MS/MS of peptides in an ICR cell found that increasingly larger peptides can be dissociated in similar time scales, despite the expected increase in kinetic shift for larger ions, with the conclusion that larger ions have more efficient energy transfers. The measured efficiency for the small peptide gly-gly-ile was 42% [15, 17a, b]. (2) Trajectory calculations showed that this efficiency increases to ca. 90% for the nonapeptide bradykinin and it was concluded that the energy transfer efficiency to peptides increases as the ions increase in size [15, 17a]. (3) Trajectory calculations by Merouch and Hase [18] showed that the energy transfer to peptides in head-on collisions (impact parameter $b = 0$) increases with the peptide size, and is similar to that of an impulsive model, given approximately by

$$\frac{\Delta E_{\text{int}}}{E_{CM}} = \frac{4 m_2 m_3 (m_2 + m_1)(m_1 - m_3)}{(m_2 + m_3)^2 m_1^2} \qquad (3)$$

where E_{CM} is the center-of-mass translational energy, and m_3 is a fit parameter (m_3 = 74, 101, and 155 for Ne, Ar, and Kr at E_{CM} = 4.35 eV). In the limit that the ion mass m_1 becomes very large, the energy transfer efficiencies for Ne, Ar, and Kr are calculated to be 0.67, 0.81, and 0.90. (We provide experimental evidence below that the energy transfer efficiencies for Ne, Ar, and Kr are nearly the same for large protein ions). (4) Measurements of the efficiency of conversion of center-of-mass translational energy to internal energy for peptide dimers of mass ca. 1000 in collisions with Ar at energies E_{CM} of 1.6 to 7.7 eV showed average efficiencies of 81 ± 40% or 102 ± 34% when the experimental data were interpreted with the kinetic method and RRKM theory respectively [19]. Although the uncertainties are large, the efficiencies are high. Extrapolation of all of these results from peptides to proteins suggest the energy transfer efficiencies will be very high. (5) A detailed study of the energy losses of protein ions passing through the collision cell of a triple quadrupole system concluded that the best description of collisions between protein ions and rare gases corresponds to diffuse scattering [16]. In diffuse scattering the ion and neutral collide, and the collision partners separate in the center of mass system with a kinetic energy determined by the surface temperature of the protein. For center-of-mass energies of about 1 eV which are used in our triple quadrupole experiments, this corresponds to highly inelastic collisions ($\phi > 0.90$). In the calculations below, we use ϕ = 1.0 in eq 2. If better estimates of ϕ become available, the results from eq 2 can be scaled accordingly.

Simulation of Ion Activation and Dissociation

The above discussion of kinetic shifts illustrates the orders of magnitude for the internal energies, lab energies and time scales involved in MS/MS of protein–protein complexes. It is simplistic because ions lose energy as they move through the collision cell, the rate constant for dissociation increases as ions move through the collision cell gaining internal energy, and the place where the reaction occurs is not well defined. To gain further insights, the activation and dissociation of an ion of mass 23,000 (similar to cytochrome c–cytochrome b_5 complexes) in collision with Ar was simu-

lated in a spread sheet calculation. A mean free path of 0.1515 cm was used, the ion was given an initial internal energy of 229 eV (i.e., thermal at 295 K), and the rate constant for dissociation was modeled by eq 1 with $v = 10^9$, $E_0 = 0.5$ eV, and $s = 8994$, as above. In this simulation, the ion travels 0.1515 cm into the cell with its initial kinetic energy and has a first collision. It is assumed that all the center-of-mass energy is transferred to internal energy, so the ratio of translational energy after a collision T', to the energy before the collision T, is given by

$$\frac{T'}{T} = \frac{m_1^2}{(m_1 + m_2)^2} \tag{4}$$

The time between collisions is given by $t = \lambda/v$ where v is the ion speed in the lab frame $\left(v = \sqrt{\frac{2T}{m_1}}\right)$. The probability of **not** reacting in the time between entering the cell and the first collision is given by

$$\bar{P}_r^0 = \exp(-k(E_{\text{int}})t) \tag{5}$$

In the first collision the ion gains an internal energy equal to the center-of-mass energy; this is added to the internal energy. After the first collision the ion has a new, slightly reduced lab energy and travels 0.1515 cm before having a second collision. The time to travel this distance is calculated, and the probability of **not** reacting between the first and second collisions, $\bar{P}_r^1$, is again calculated from eq 5. The cumulative probability of not reacting between entering the cell and the first collision, and between the first and second collisions is $\bar{P}_r = \bar{P}_r^0 \cdot \bar{P}_r^1$. This process is repeated for 131 collisions, at which point the ion is at the cell exit (cell length 20 cm). The cumulative probability of reaction at any point in the cell is $P_r = 1 - \bar{P}_r$. The simulation was run for different injection energies from 100 to 2000 eV. Figure 1 shows the calculated cumulative probability of reaction by the time ions reach the cell exit versus the lab translational energy at the cell entrance. The curve has a shape similar to the experimental curves below. In this model the reaction yield is 50% when the initial ion lab energy is 1203 eV. Figure 2a shows the increase in ion internal energy as it moves through the cell under conditions that give 50% reaction at the cell exit. The ion accumulates internal energy through 131 collisions. The increase is not linear because ions lose translational energy as they travel through the cell. In this case, with an initial laboratory translational energy of 1203 eV, the ion translational energy at the cell exit is 763 eV.

Figure 2b shows the rate constant for dissociation versus distance in the cell. Because the rate increases very rapidly with energy, the rate constant changes by four orders of magnitude as ions pass through the cell. The cumulative yield of product ions at each point in the cell is shown in Figure 2c for injection energies of 765, 1203, and 1584 eV, which correspond to product

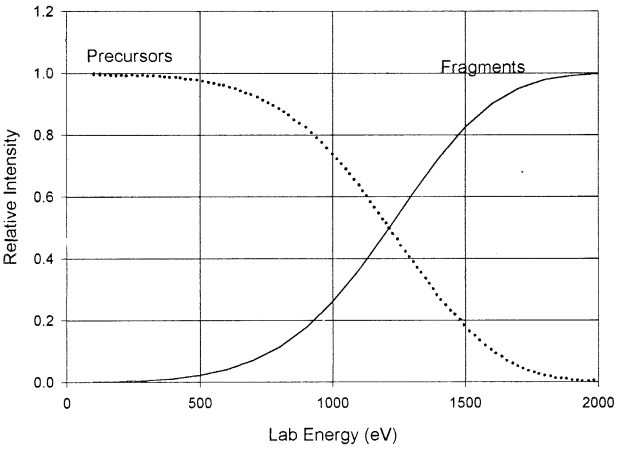

Figure 1. Calculated loss of precursor ions and formation of product ions for a complex of mass 23,000 with collision cross section 2000 Å^2, passing through a collision cell with Ar at 1.0 mtorr. Ions accumulate internal energy in 132 collisions.

yields at the cell exit of 10, 50, and 90% respectively. Figure 2c shows that almost all of the reaction occurs in the second half of the cell. Under conditions where the reaction yield is 50%, the reaction takes place mostly in the last 5 cm of the cell.

The simple RRK expression for the rate is not intended to be an accurate description for protein–protein complexes. It is used here as a simple analytical expression in which the rate increases rapidly with energy. The simulation in Figure 2c was repeated for frequency factors v from 10^8 to 10^{14}, dissociation energies E_0 of 0.2 to 1.0 eV, and numbers of effective oscillators s from 3000 to 9000. In all cases the reaction takes place near the cell exit (data not shown). For any reasonable rate model, the rate increases so rapidly with energy that it is the ions near the cell exit that have accumulated the most internal energy that contribute to the fragmentation. An exception to this relationship occurs if the ions already have sufficient internal energy from the source when they are at the cell entrance to dissociate throughout the cell.

To calculate the internal energy added to ions from eq 2, it is necessary to choose a length l where the ions react. The calculations below assume $l = 18$ cm. Figure 2c show this is an approximation, because the reaction occurs over a distance of ca. 4–5 cm. If eq 2 is used to calculate ΔE_{int} from the computer "experiment" of Figure 2 with $l = 18$ cm, it gives $\Delta E_{\text{int}} = 199$ eV. The value in the simulation at 18 cm is 202 eV and ranges from 183 eV at 16 cm to 220 eV at 20 cm. Note that the energy calculated from eq 2 is independent of any assumptions about the rate energy curve.

The simulation has been improved with a full Monte Carlo simulation of the number of collisions, the scattering angles, and the energies transferred to the ion (with an average energy transfer of 90% of the center-of-mass energy). Results from the simple model represented by eq 2 match the calculated internal energies of

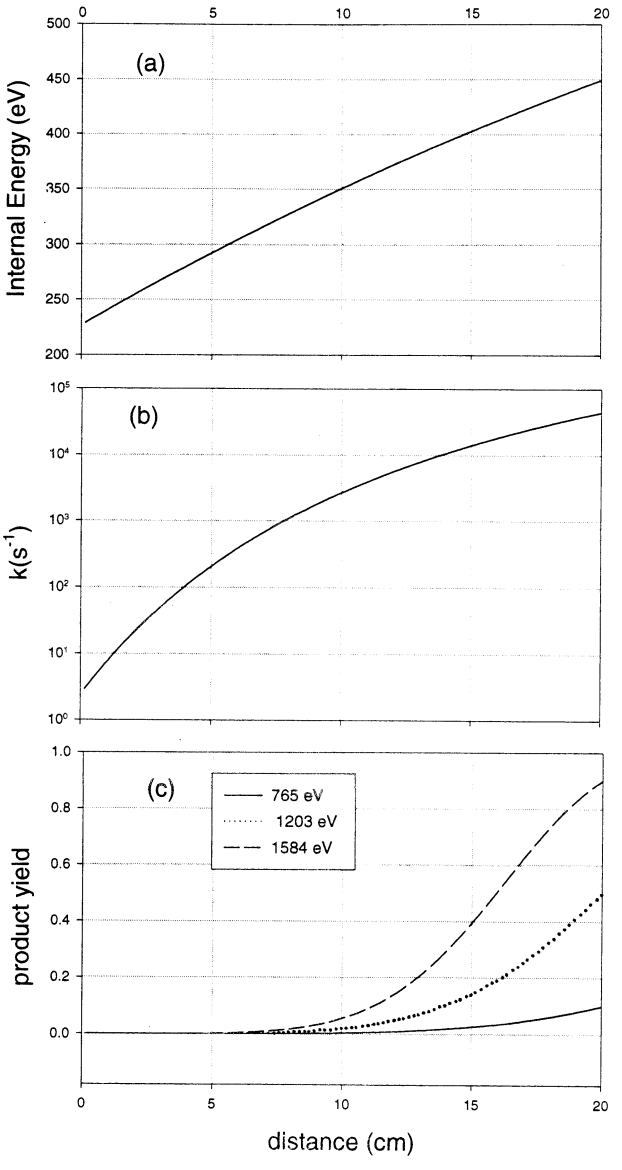

Figure 2. (**a**) Internal energy gained by an ion of mass 23,000 versus distance traveled, as it passes through a collision cell with 132 collisions with Ar. (**b**) Rate constant for dissociation versus distance traveled in the collision cell. (**c**) Product yield versus distance as a precursor ion travels through a collision cell. The initial energies were 765, 1203, and 1584 eV. The curve for 1203 eV corresponds to a 50% yield of products.

ions in the full simulation for a wide range of rate parameters within about 10% [20].

Experimental

Tandem Mass Spectrometry

Experiments were done with the triple quadrupole system shown in Figure 3. Ions from a pneumatically assisted electrospray source (solution flow rate 1 μL min^{-1} in all experiments) pass through a dry nitrogen "curtain" gas, a sampling orifice, a skimmer, and into a radio frequency (RF) only quadrupole, Q0, which acts

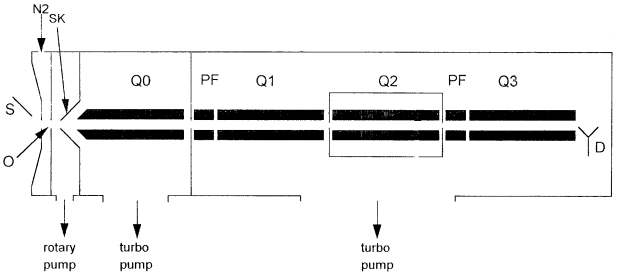

Figure 3. Schematic of the ESI-triple quadrupole mass spectrometer system. S, electrospray ionization source; N2, nitrogen "curtain" gas; O, sampling orifice; SK, skimmer; Q0, RF-only quadrupole; PF, prefilter (short RF-only quadrupole); Q1, mass-analyzing quadrupole; Q2, RF-only quadrupole/collision cell; Q3, mass-analyzing quadrupole; D, detector.

as an ion guide. Collisions in Q0 cool ions to translational energies of 1–2 eV [9]. Ions then pass through an inter-quadrupole differential pumping aperture, a short RF only quadrupole and into a mass analyzing quadrupole Q1. Ions enter the collision cell, which contains an RF only quadrupole Q2, with energies determined by the difference between the rod offsets of Q0 and Q2. The pressure in the collision cell was measured with a precision capacitance manometer (MKS Baratron type 120 high-accuracy pressure transducer, MKS, Andover, MA, USA), manufacturer's stated accuracy 0.12% of reading. The precursor ion was mass selected in the first quadrupole, Q1, and was collisionally activated and dissociated in Q2 to produce product ions which were mass analyzed in quadrupole Q3. The RF voltages of all the quadrupoles were phase locked with zero phase shift. The detector, D, was operated in ion counting mode. An orifice–skimmer voltage difference of 50 V was used in the MS/MS experiments. The collision energy of precursor ions was systematically increased, and the dissociation voltage (i.e., difference in voltage between the Q0 and Q2 offsets giving 50% relative yield of product ion) of each precursor ion was determined at four different pressures of argon in the range 0.50–1.5 mtorr. In some experiments the collision gas was Ne or Kr at 1.00 mtorr.

Tryptic bovine liver cytochrome b_5, yeast iso-1-cytochrome c Cys102Thr and its trimethyl-Lys72Ala (J72A), Lys73Ala (K73A), Lys79Ala (K79A), and Lys87Ala (K87A) variants were prepared and purified as in [21]. All yeast cytochrome c samples carried a Cys102Thr substitution. This substitution prevents intermolecular disulphide bond formation and greatly reduces the rate of autoreduction without affecting the structural or functional properties of the protein. Equal volumes of 20 μM protein solutions in water were mixed to produce complexes. Methanol (HPLC grade, Fisher Scientific, Nepean, ON) was added (10% vol/vol) to these mixtures to improve the spray efficiency. Mass spectra of cytochrome c–cytochrome b_5 complexes and the corresponding individual proteins were recorded at an orifice-skimmer voltage difference of 50 V. The mass

spectrum of the complex at an orifice-skimmer voltage difference of 100 V was also recorded. Complexes of cytochrome b_5 and other cytochrome *c* mutants can also be observed by this procedure.

All gases were from Praxair (Richmond, BC, Canada) with manufacturer's stated purities Ne, UHP grade (99.996%), Ar, Linde grade (99.9995%), Kr, research grade (99.996%), nitrogen, UHP grade (99.999%).

Collision Cross Section Measurements

Collision cross sections of cytochrome b_5, cytochrome *c* and the complex ions were measured by the energy loss method described previously [16]. Drag coefficients for diffuse scattering were used. The collision gas was neon. Ions were injected into the collision cell with an energy of 10 eV per charge. At this collision energy no dissociation of the complex occurred. The orifice-skimmer voltage difference was 50 V, the same as that used for MS/MS experiments. Collision cross sections for the complex ions +10 and +11 at a 100 V orifice-skimmer voltage difference were also measured. Collision cross sections for other gases were calculated from the measured cross sections with Ne and the atomic radii of Ar and Kr as described in [16]. These cross sections were 2.9% and 3.3% greater, respectively, than those with neon.

Results and Discussion

Spectra and Formation of Complexes

Mass spectra of cytochrome *c*, cytochrome b_5, and the cytochrome *c*–cytochrome b_5 complex are shown in Figure 4. In Figure 4c, four charge states of the complex ions, +10 (*m/z* 2280), +11 (*m/z* 2073), +12 (*m/z* 1900), and +13 (*m/z* 1754) were produced. The charge state +9 (*m/z* 2533) of the complex could not be resolved from overlapping peaks of charge state +5 (*m/z* 2542) of cytochrome *c* and probably +4 (*m/z* 2520) of cytochrome b_5 as well. Figure 4a and b are mass spectra of cytochrome *c*, and cytochrome b_5, respectively. Deconvolution of these mass spectra gave the following molecular weights: cytochrome *c*, 12,710 ± 1, cytochrome b_5, 10,080 ± 1, and cytochrome *c*–cytochrome b_5, 22,790 ± 2. These molecular weights were obtained by averaging three separate measurements on three separate days and are consistent with the sequences of the proteins.

Figure 4c shows that the noncovalent complex of cytochrome *c* and cytochrome b_5 can be detected by ESI-MS. Note the *m/z* scale in Figure 4c and d is different from that of Figure 4a and b, and this causes the peaks to appear broader. From the solution equilibrium constant, the proteins are calculated to be more than 90% complexed. However, the relative abundance of the complex ions in the mass spectrum is less than 15%, much lower than expected from the solution equilibrium. The lower abundance may result from a

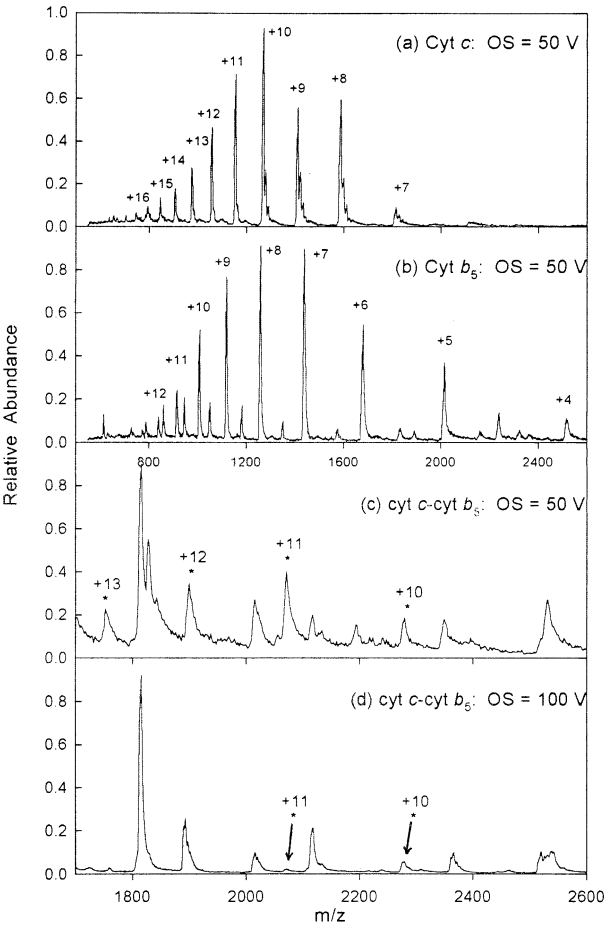

Figure 4. Mass spectra of (**a**) cytochrome *c*, (**b**) cytochrome b_5, (**c**) complexes of cytochrome *c*–cytochrome b_5, and (**d**) complexes of cytochrome *c*–cytochrome b_5. In (**a**), (**b**), and (**c**) the orifice-skimmer voltage difference was 50 V. In (**d**) it was 100 V.

shift in pH in the spray process [22], the addition of 10% methanol to the solution, or dissociation of the complexes in the orifice-skimmer region of the mass spectrometer. Figure 4c also shows peaks from cytochrome *c* bound to two cytochrome b_5 molecules at *m/z* = 2192 (+15) and at *m/z* 2348 (+14). This trimer was proposed in early work but a critical review of the evidence concluded it is not formed in solution [10]. The low abundance of the complex ions and the formation of nonspecific trimer complexes show that the mass spectrum does not reflect the solution equilibria, and it is possible that the cytochrome *c*–cytochrome b_5 complexes are not formed by a process which involves their specific solution interactions. However, for the detailed testing of the collision model described below, this is not important.

Comparison of mass spectra at different orifice-skimmer voltages (Figure 4c and d) shows that when a 50 V orifice-skimmer (OS) voltage difference was applied, the charge state distribution from +10 to +13 for the complex could be observed, and all four charge states showed considerable intensities. An orifice-skimmer voltage lower than 50 V resulted in a low signal

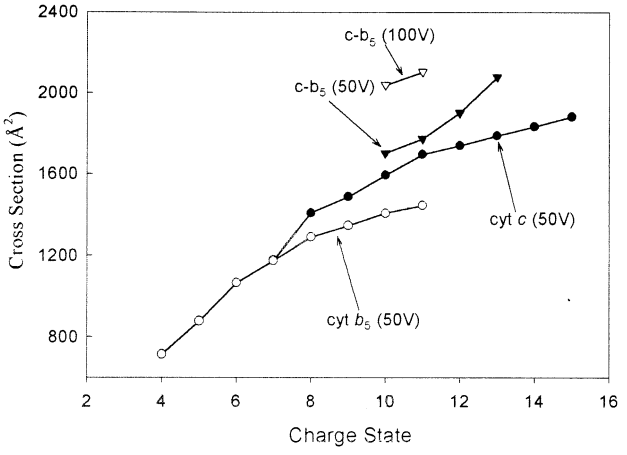

Figure 5. Collision cross sections of cytochrome c, cytochrome b_5, and the cytochrome c–cytochrome b_5 complex. The collision gas was Ne. The voltage value shown on the figure refers to the orifice-skimmer voltage difference. "c–b_5" indicates the cytochrome c–cytochrome b_5 complex.

intensity and poor signal-to-noise (S/N) ratio. When the orifice-skimmer voltage difference was increased to 100 V, only the charge states +10 and +11 of the complex survived and with low abundance. This result was obtained because the lower charge states of the complexes require greater internal energy to induce dissociation (confirmed by MS/MS, see below). The peak at m/z 1893 in Figure 2d arises from apo-cytochrome b_5^{+5} that is produced by the dissociation of holo-cytochrome b_5; (cytochrome b_5 contains a noncovalently bound heme group). Thus, the observation of this intact noncovalent complex by ESI-MS requires a balance between interface conditions to provide sufficient energy for ion desolvation, while preventing the dissociation of the complexes.

The charge state distributions for cytochrome c–cytochrome b_5 complexes (including those variants studied here) have 4–5 charge states from +10 (or +9) to +13. Compared to the individual proteins, these complex ions show relatively low charge states and narrow charge state distributions. It has been suggested that this may be a common attribute for all protein–protein complexes [23]. Multiply charged ions of intact noncovalent complexes such as protein–protein complexes often exhibit a narrow distribution of relatively low charge states [1a].

Collision Cross Sections

Collision cross sections with Ne for cytochrome c, cytochrome b_5 and the complex ions are shown in Figure 5. The measurements were done at an orifice-skimmer voltage difference of 50 V for the proteins and 50 V and 100 V for the complex. The cytochrome c cross sections are about 10% greater than earlier measurements in this lab [16]. The difference may be due to the different sequence and higher molecular weight of the yeast iso-1-cytochrome c used here (m.w.12,700 versus

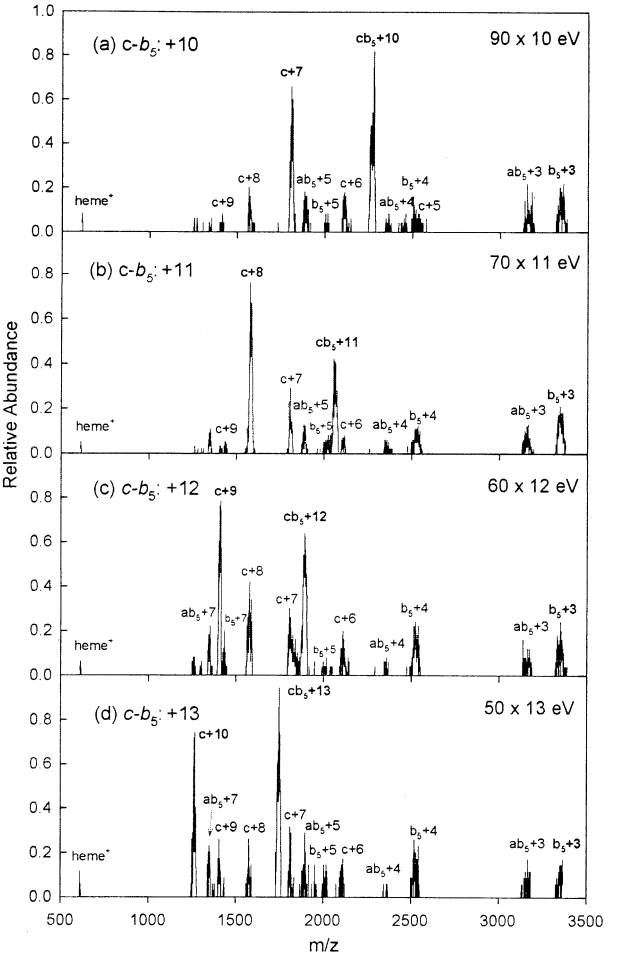

Figure 6. Tandem mass spectra of cytochrome c–cytochrome b_5 complex ions. c, b_5, ab_5, and c–b5 or cb_5 represent cytochrome c, cytochrome b_5, apo-cytochrome b_5, and cytochrome c–cytochrome b_5 noncovalent complexes, respectively. The collision gas was 0.50 mtorr krypton. The injection energies are shown in the figures.

12,360) and combined uncertainties of the experiments. For a given charge state, the complex ions at an orifice-skimmer voltage difference of 50V have cross sections only slightly greater than those of cytochrome c suggesting compact structures for the complex. Cross sections increase with charge state. This increase is usually attributed to Coulombic repulsion in the ions [9b, 24a]. The cross sections for the complex at an orifice-skimmer voltage difference of 100 V are greater than at 50 V. The greater cross sections at 100 V are attributed to heating of the complexes in the orifice-skimmer region which causes the complexes to unfold. A similar effect has been reported for ions of the noncovalent complex holomyoglobin [24b].

MS/MS Spectra and Charge States of Fragments

Tandem mass spectra of charge states +10 to +13 of cytochrome c–cytochrome b_5 complex ions are shown in Figure 6. The collision gas was Kr and the ion injection

energies are shown in the figure. The results show that each charge state of the complex ions was fragmented to several pairs of cytochrome *c* and cytochrome b_5 ions. The appearance of apo-cytochrome b_5 ions and heme$^+$ in the tandem mass spectra shows that the product ions of the cytochrome *c*–cytochrome b_5 complex, holo-cytochrome b_5^{+j} can be fragmented further to apo-cytochrome $b_5^{+(j-1)}$ and heme$^+$. Previously, Hunter et al. [3b] have studied the heme-binding in several variants of cytochrome b_5 by CAD in the orifice-skimmer region.

In these ion pairs, fragment ion, cytochrome b_5, has a charge state distribution from +1 (+1 and +2 cannot be seen because of the limited *m/z* range of the mass spectrometer) to +5 with the maximum intensity at +3. The other fragment ion, cytochrome *c*, shows a charge state distribution from +5 to +10 with the maximum at the charge state +(k−3), where k is the charge state of the precursor ion. That is, with an increase of the charge state of the precursor ions, the charge state of the cytochrome b_5 ions with maximum abundance remains unchanged, while the charge state of the cytochrome *c* ions with the maximum abundance shifts from +7 to +10. Therefore, the most probable channel in the fragmentation of cytochrome *c*–cytochrome b_5 complex ions is the reaction {cytochrome *c*–cytochrome b_5}$^{+k}$ → cytochrome $c^{+(k-3)}$ + cytochrome b_5^{+3}. It has been suggested that the charge states of fragments give insights to the charge site in the complex [25]. Thus, if charges do not move in the CAD process, the charges in this complex are distributed mainly on the cytochrome *c*, whereas the cytochrome b_5 surface maintains a relatively low and unperturbed charge state distribution. This is plausible given the much more basic nature of cytochrome *c*, but remains unproven. Recently Verluis et al. [26] have described the MS/MS spectra of the dimer ion (cytochrome *c*–cytochrome *c*)$^{+11}$. Unexpectedly, the fragments showed an asymmetric charge distribution with the major channel being (cytochrome *c*–cytochrome *c*)$^{+11}$ → cytochrome c^{+8} + cytochrome c^{+3}. Asymmetric charge distributions were also seen in the dissociation of ions of streptavidin tetramers [23b]. These asymmetric distributions for cytochrome *c* dimers and streptavidin suggest that charges may move in the CAD process and this may be related to the electrostatic repulsion of the fragment ions. If the reverse reaction is considered, there will be a Coulomb barrier with a height proportional to the product of the charges on the fragment ions. For dimers, this is minimized for the most asymmetric distribution and if this Coulomb barrier contributes to the activation energy for dissociation, the most asymmetric charge distributions will have the lowest energies for dissociation. Competing with this effect, however, is the additional energy required to move charges to new sites in the complex prior to dissociation.

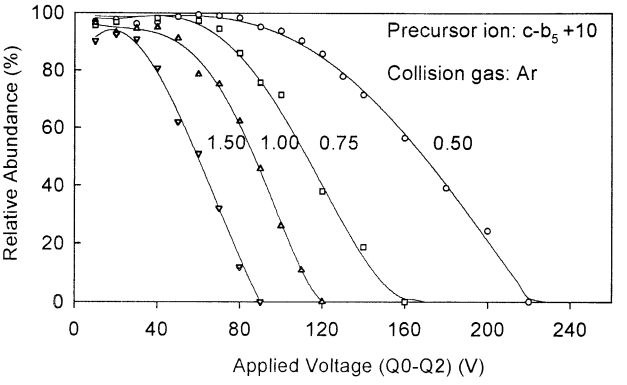

Figure 7. Relative abundance of the cytochrome *c*–cytochrome b_5 complex +10 at four different cell pressures from 0.50 to 1.50 mtorr Ar versus injection voltage (Q0–Q2). The number beside each curve is the cell pressure in mtorr.

Dissociation Voltages at Different Pressures

From tandem mass spectra of different charge states of the complex at different voltage differences between Q0 and Q2, the relative abundance of the precursor ion was calculated as $I_p/I_p+\Sigma_{i=1}^{j}I_{frag}$, where I_p is the area of the peak of the precursor ion, i.e., the complex ion with subtraction of the background; and $\Sigma_{i=1}^{j}I_{frag}$ is the sum of the areas of the peaks of all fragments. A plot of these relative abundances against the Q0–Q2 voltage difference gives a curve, which is defined as the dissociation curve. The dissociation curves for the complex cytochrome *c*–cytochrome b_5^{+10} at 0.50, 0.75, 1.00, and 1.50 mtorr of argon collision gas are shown in Figure 7. Dissociation curves for the other charge states +11, +12, and +13 at these four cell pressures are similar (data not shown).

Dissociation voltages for the cytochrome *c*–cytochrome b_5 complex ions +10 to +13, at four different cell pressures of Ar between 0.50 and 1.50 mtorr are shown in Figure 8. Higher pressures result in lower dissociation voltages because ions have a greater num-

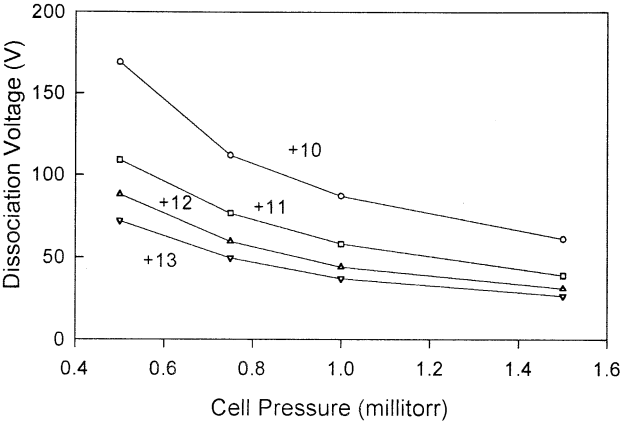

Figure 8. The dissociation voltages of the cytochrome *c*–cytochrome b_5 complex ions with charges from +10 to +13 at four different cell pressures over a range of 0.50–1.50 mtorr. The collision gas was Ar.

Table 1. Internal energies (eV) required to dissociate cytochrome c–cytochrome b_5 complex ions at four different pressures of argon

P (mtorr)	+10	+11	+12	+13
0.50	140	103	97	94
0.75	132	103	93	89
1.00	131	99	87	83
1.50	125	90	84	81

ber of collisions. However this is not a linear relationship because energy losses of ions moving through the cell must be considered and energy losses are greater at higher pressures. Figure 8 shows that the dissociation voltage for each charge state of the ions decreases by a factor of ca. 2.5 when the pressure is increased by a factor of 3 (from 0.50 to 1.50 mtorr). The dissociation voltage cannot be directly used to compare the relative stability of different ions because ions have different charge states and also different cross sections which give different numbers of collisions and different energy losses at a given cell pressure.

Internal Energies and Reaction Times

The additional internal energy, ΔE_{int}, added to the ions at each pressure was calculated from the collision model described earlier (eq 2 with l = 18 cm and ϕ = 1.0) with the results shown in Table 1. The ca. 2.5-fold spread in dissociation voltages apparent in Figure 8 is reduced to about a ±6% spread about the mean or a 12% difference between the largest and smallest for a given charge state (expressed as a fraction of the largest number). Simplistically, a given ion should require the same energy to cause dissociation in different experiments. Thus eq 2 can account for most of the differences in internal energy for experiments over a broad range of collision energies and pressures. There are, however, systematic decreases in ΔE_{int} at higher pressures, as discussed below.

Dissociation Voltages with Different Gases

The +10 ions of the complex were dissociated in collisions with Ne, Ar, and Kr at 1.00 mtorr. Dissociation curves derived from this work are shown in Figure 9. The dissociation voltages are 175 V, 87 V, and 41 V for Ne, Ar, and Kr, respectively. For a given pressure, heavier gases require lower dissociation voltages because the center-of-mass energy is higher for a given lab energy. Added internal energies calculated from eq 2 with l = 18 are 142, 131, and 107 eV for Ne, Ar, and Kr, respectively. Thus the ca. 4-fold difference in dissociation voltages is reduced to a ca. 30% spread in added internal energy. As in experiments at different pressures, the collision model accounts for most of the variation in voltage. However as with experiments at higher pressures, there is a systematic decrease in the calculated ΔE_{int} values as the mass of the collision gas increases.

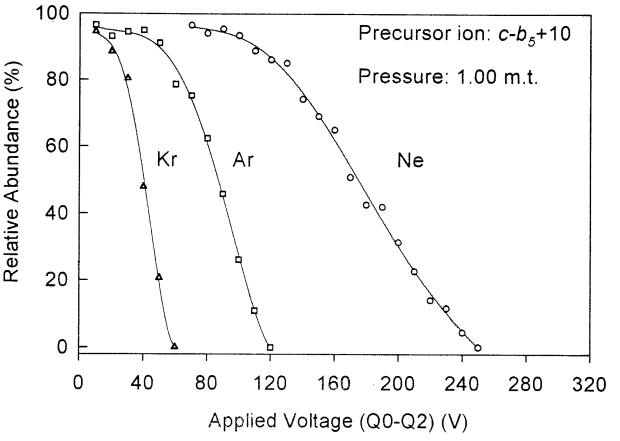

Figure 9. Relative abundance of the cytochrome c–cytochrome b_5 complex +10 at 1.00 mtorr of different collision gases, Ne, Ar, and Kr, versus injection voltage.

Internal Energies and Reaction Times

We attribute the systematic decrease in the calculated ΔE_{int} values at higher pressures or with heavier gases to an increased time available for reaction. As discussed, experiments at higher pressures or with heavier gases result in lower dissociation voltages. Thus, ions move more slowly through the cell, have longer times to react and require somewhat less internal energy to give a 50% product yield. This argument can be made at least semi-quantitative. Consider the +10 ions. The ion speed near the cell exit (at 18 cm) can be calculated from the translational energy at this point. This energy is less than the injection energy and is given by

$$\frac{E}{E^0} = \exp\left(-\frac{C_D n m_2 \sigma l}{m_1}\right) \quad (6)$$

with l = 18 cm. The reaction takes place over ca. 4 cm (from l = 16 to l = 20 cm). For the experiment with Ar at 0.5 mtorr, the initial energy is 10 ×169 = 1690 eV, the translational energy at l = 18 cm is 1350 eV and the time to travel the last 4 cm of the cell is calculated to be 11.7 μs. For the experiment at 1.5 mtorr of Ar, the initial injection energy is 10 × 61 = 610 eV, the translational energy at l = 18 cm is 268 eV and the time available for reaction is 23.8 μs. For each pressure or collision gas, the reaction time and energy input ΔE_{int} can be calculated. For the +10 ion, Figure 10 shows the values of ΔE_{int} calculated from eq 2 versus the time available for reaction. There is a systematic decrease in ΔE_{int} for longer reaction times, as expected for a unimolecular reaction. Experiments with different gases at 1.00 mtorr yield nearly the same curve as experiments with Ar at different pressures. For example, Ar at 0.5 mtorr and Ne are 1.0 mtorr happen to result in nearly the same time

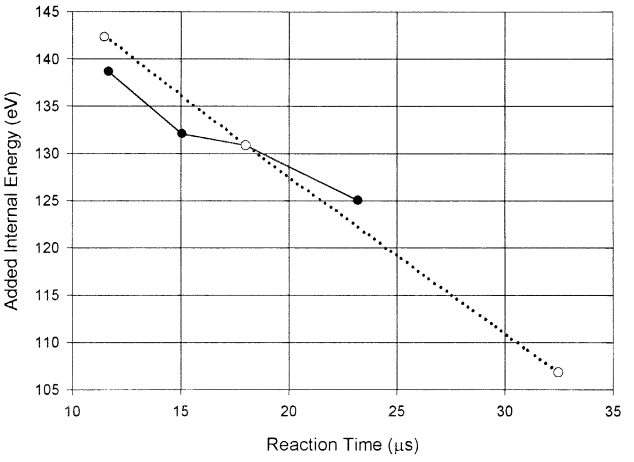

Figure 10. The internal energy that must be added to the +10 complex ions to induce reaction versus the time available for reaction. The solid circles are from experiments at four different pressures and the open circles are from experiments with Ne, Ar, and Kr at 1.0 mtorr.

for reaction, 11.7 and 11.5 μs respectively, and give nearly identical ΔE_{int} values (140 and 142 eV respectively). Experiments with different gases have a greater spread in calculated values of ΔE_{int} because they occur over a greater range of times. Because the data for Ne and Kr fall on the same curve as the data for Ar at different pressures, it appears that Ne, Ar, and Kr all have similar energy transfer efficiencies, ϕ.

The same analysis was applied to the other charge states, with the results shown in Figure 11. It is apparent that experiments with different charge states have different reaction times, even for the same collision cell pressure. For example, at 0.50 mtorr the calculated reaction times are 11.7, 13.9, 14.9, and 16.0 μs for the +10 to +13 ions, respectively. The best determination of the energy that must be added to induce reaction comes from comparing equal reaction times. For reaction times of 20 μs, for example, ΔE_{int} values interpolated from

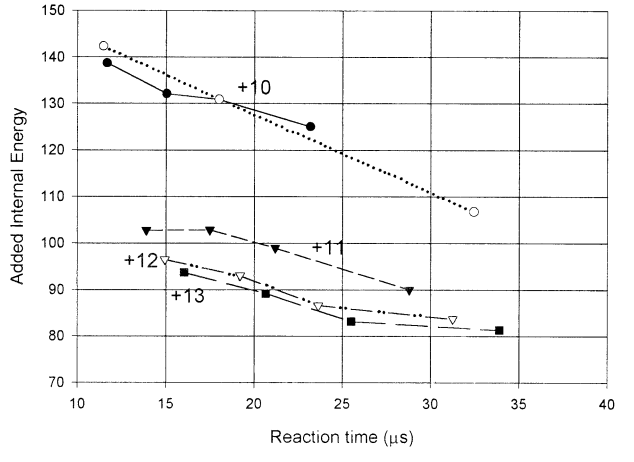

Figure 11. The internal energy that must be added to the complex ions to induce reaction versus the time available for reaction. The points for the +10 ion are taken from Figure 10.

Figure 11 are 128, 100, 92, and 90 eV for the +10 to +13 ions. The data in Figures 10 and 11 could also be displayed as approximate rate constant versus added energy curves, although for a very limited range of energies. To give a 50% reaction yield in time t requires a rate constant $k = -\ln(0.50)/t$. Unfortunately, the internal energy that the ions have before entering the collision cell is unknown, so this is not a true rate energy curve.

Figure 11 shows that compared to the +10 ion, the +11, +12, and +13 ions require less added energy to dissociate in a given time. It is likely the added charges contribute to destabilizing the complex. There may also be a contribution from additional heating of the more highly charged ions in the ion sampling region. The energy added to an ion in collisional activation in the orifice-skimmer region is proportional to its charge [27]. However the comparatively large decrease in ΔE_{int} in going from +10 to +11 ions, followed by a smaller decrease in going to +12 and nearly identical values for +12 and +13 ions show that this is not the only reason for the differences between charge states.

Experiments with Cytochrome c Variants

Chemical modifications of surface residues on cytochrome *c* and the effect of these modifications on the reaction of cytochrome *c* derivatives with other proteins have been reviewed by Millet and Durham [28]. The surface lysine residues on the cytochrome *c* such as Lys73, Lys79, Lys86, Lys87, and trimethyl-Lys72 etc. are of structural and functional significance. The lysine residues at these positions are located in the binding domain of cytochrome *c*. They play an important role in the electron transfer reaction with other proteins such as cytochrome *c* oxidase and cytochrome b_5 [28]. The replacement of one or more of these lysine residues on the surface of cytochrome *c* by another amino acid can, in principle, reveal the binding sites or the contribution of individual lysines to binding. The trimethyl-Lys72Ala (J72A), Lys73Ala (K73A), Lys79Ala (K79A), and Lys87Ala (K87A) variants of yeast iso-1-cytochrome *c* have been described elsewhere [11, 21a, c, 29]. These variants were found to have similar pK_a (wild type, 8.70; Lys73Ala, 8.82; Lys79Ala, 8.44; Lys87Ala, 8.47) and similar reduction potentials and thermal stability [29]. These substitutions only slightly destabilize the complex in solution. The association constants, K_A, for the complex with wild type, trimethyly-Lys72Ala, and Lys79Ala cytochrome *c* at pH 6.00 and an ionic strength of 10 mM are $2.09 \pm 0.19 \times 10^6\ M^{-1}$, $1.23 \pm 0.15 \times 10^6\ M^{-1}$, and $1.40 \pm 0.16 \times 10^6\ M^{-1}$ respectively [30]. Association constants for the Lys73Ala and Lys87Ala variants have not been measured. However these latter substitutions are expected to have less effect on the K_A values than changes at positions 72 and 79 [10].

Ions of complexes of cytochrome b_5 with the trimethyl-Lys72Ala, Lys73Ala, Lys79Ala, or Lys87Ala mu-

tants of yeast iso-1-cytochrome *c* were produced in the gas phase with the same procedures used to produce the complex of cytochrome b_5 and wild type iso-1-cytochrome *c*. ESI mass spectra of these mutant complexes at an orifice-skimmer voltage difference of 50 V are very similar to those of the wild type proteins (Figure 4c and d). Similar to the wild type protein complex, all of these mutant complexes have the same charge state distribution, +10 to +13, even though they contain one less basic residue. Deconvolution of these spectra gave molecular weights of 22,685 ± 2 for trimethyl-Lys72Ala–cytochrome b_5 complex and 22,728 ± 2 for Lys73Ala–cytochrome b_5, Lys79Ala–cytochrome b_5, and Lys87Ala–cytochrome b_5 complexes, indicating that all of these cytochrome *c* mutants react with cytochrome b_5 to form the noncovalent complex with a stoichiometry of 1:1. The relative abundance of complex ions with variants is ca. 15%. This again is lower than expected from the solution equilibrium, but similar to the wild type proteins.

Collision Cross Sections of Cytochrome c Variants and Complexes

Collision cross sections with Ne for the trimethyl-Lys72Ala, Lys73Ala, Lys79Ala, and Lys87Ala mutants of yeast iso-1-cytochrome *c* and the corresponding cytochrome *c*–cytochrome b_5 complexes were measured. The difference in cross sections between wild type cytochrome *c* and mutant cytochrome *c* for a given charge state is less than 6%, and less than 4% for their complexes. The precision of cross section measurements is typically ±3%. Thus, there are no significant effects of mutations on collision cross sections for all cytochrome *c* mutants and the corresponding noncovalent complexes. This finding indicates that the replacement of trimethyl lysine residue at position 72, or one of the lysine residues at positions 73, 79, and 87 by an alanine residue does not have a large effect on the conformation of cytochrome *c* or cytochrome *c*–cytochrome b_5 complexes. Recently, Pollock et al. [21c] studied the trimethyl-Lys72Ala variant of yeast iso-1-cytochrome *c* and found that trimethylation of Lys72 has no effect on the structural stability of cytochrome *c*. The dimethyl derivatives of horse and yeast cytochrome *c*, i.e., N, N-dimethyl-lysine cytochrome *c*, were characterized for use as NMR probes of the complexes formed by cytochrome *c* with cytochrome b_5 and yeast cytochrome *c* oxidase by Moore et al. [31]. These authors concluded that the electrostatic properties and structures of the derivatized cytochromes are not significantly perturbed by the dimethylation of lysine residues; neither are the electrostatics of protein–protein complex formation or rates of interprotein electron transfer. The same charge state distribution for wild type and variant complexes and the similar cross sections for wild type and different variants in the present work show that the conformations of the cytochromes and the corresponding complexes in the gas phase are not greatly affected by these mutations.

Table 2. Added internal energies (eV) to dissociate complexes of wild type and variant cytochrome *c*–cytochrome b_5 in 20 μs

Protein	+10	+11	+12	+13
w.t. cyt c–b_5	128	100	92	90
J72A cyt c–b_5	132	100	89	84
K73A cyt c–b_5	131	101	91	94
K79A cyt c–b_5	136	103	96	96
K87A cyt c–b_5	133	104	95	93

Comparison of Dissociation Voltages and Internal Energies Required for the Dissociation of Complexes Between Cytochrome b_5 and Cytochrome c Variants

Dissociation voltages for all charge states of the complexes of various cytochrome *c* variants with cytochrome b_5 in collisions with Ne, Ar, and Kr were measured by tandem mass spectrometry. For each charge state of each variant complex, a graph of ΔE_{int} versus reaction time was constructed for the data from the three gases (similar to Figure 10 for the wild type proteins). The added internal energies necessary to induce reaction in 20 μs were interpolated from the graphs and are shown in Table 2. For a given charge state, the energies are the same within a few percent for the different variants, and the decreases in energy with increasing charge on the complex are very similar.

Relative Stability of Complexes of Various Mutants

Table 2 shows that for all cytochrome *c*–cytochrome b_5 complexes the charge state +10 is more stable than higher charge states, and the other three charge states show similar stability. However, for a given charge state of the different variant complexes the energies required for the dissociation of complexes in the gas phase were found to be similar. This demonstrates that the mutations do not cause detectable perturbations to the formation, conformation, and stability of the cytochrome *c*–cytochrome b_5 complex in the gas phase. This is similar to these mutant complexes in solution. However the resulting implications for the structures of the gas phase ions are inconclusive. It is possible that binding in the gas phase complexes occurs through the same residues as the solution complexes, and similar ΔE_{int} values reflect the fact that the solution binding is only slightly altered by these mutations. It is equally possible that the gas phase ions have completely different structures and the modified residues are not involved in the gas phase binding at all, so that substitutions at these sites have no effect on the gas phase binding.

Summary

This paper has examined an improved method to interpret triple quadrupole MS/MS experiments of complexes of large ions, and applied it to a study of complexes between cytochrome *c* and cytochrome b_5. Modeling of the activation and dissociation process of ions in a triple quadrupole mass spectrometer shows that most of the reaction occurs near the cell exit. Experiments at different pressures or with different gases were interpreted with a previously proposed collision model to calculate the internal energy transferred to ions to induce dissociation. Small but systematic differences under different experimental conditions are attributed to different times available for reaction. A method to correct for this was presented. Ne, Ar, and Kr were found to have similar energy transfer efficiencies.

Complexes of cytochrome *c* and cytochrome b_5 were detected in ESI spectra, but with abundances less than expected from the solution equilibrium. In MS/MS experiments, dissociation of a complex with charge +k gave as the most abundant fragments cytochrome b_5^{+3} and cytochrome $c^{+(k-3)}$. Adding charges destabilizes the gas phase complex. A series of cytochrome *c* variants with Lys residues, thought to be involved in solution binding replaced by Ala, showed no differences in the stability of the gas phase complexes. The implications for the binding in the gas phase ions are inconclusive.

Acknowledgments

This work was supported by an NSERC-SCIEX Industrial Chair (DJD), a Canada Research Chair (AGM) CIHR grant MT-14021 (AGM), and an NSERC post graduate fellowship (Y-LC).

References

1. (a) Loo, J. A. Studying Noncovalent Protein Complexes by Electrospray Ionization Mass Spectrometry. *Mass Spectrometry Reviews* **1997,** *16,* 1–23. (b) Pramanik, B. N.; Bartner, P. L.; Mirza, U. A.; Liu, Y.-H.; Ganguly, A. K. Electrospray Ionization Mass Spectrometry for the Study of Non-covalent Complexes: An Emerging Technology. *J. Mass Spectrom.* **1998,** *33,* 911–920. (c) Przybylski, M.; Glocker, M. O. Electrospray Mass Spectrometry of Biomacromolecular Complexes with Noncovalent Interactions—New Analytical Perspectives for Supramolecular Chemistry. *Angew. Chem. Int. Ed. Engl.* **1996,** *35,* 806. (d) Loo, J. A. Electrospray Ionization Mass Spectrometry: A Technology for Studying Noncovalent Macromolecular Complexes. *Int. J. Mass Spectrom.* **2000,** *200,* 175–186.
2. (a) Dunbar, R. C.; McMahon, T. B. Activation of Unimolecular Reactions by Ambient Blackbody Radiation. *Science* **1998,** *279,* 194–197. (b) Gross, D. S.; Zhao, Y.; Williams, E. R. Dissociation of Heme–Globin Complexes by Blackbody Infrared Radiative Dissociation: Molecular Specificity in the Gas Phase? *J. Am. Soc. Mass Spectrom.* **1997,** *8,* 519–524. (c) Schnier, P. D.; Klassen, J. S.; Strittmatter, E. F.; Williams, E. R. Activation Energies for Dissociation of Double Strand Oligonucleotide Anions: Evidence for Watson-Crick Base Pairing in vacuo. *J. Am. Chem. Soc.* **1998,** *120,* 9605–9613.
3. (a) Van Dorsselaer, A.; Huang, E. C.; Pramanik, B. N.; Tsarbopoulos, A.; Reichert, P.; Ganguly, A. K.; Trotta, P. P.; Nagabhushan, T. L.; Covey, T. R. Application of Electrospray Mass Spectrometry in Probing Protein–Protein and Protein–Ligand Noncovalent Interactions. *J. Am. Soc. Mass Spectrom.* **1993,** *4,* 624–630. (b) Hunter, C. L.; Mauk, A. G.; Douglas, D. J. Dissociation of Heme from Myoglobin and Cytochrome b_5: Comparison of Behavior in Solution and the Gas Phase. *Biochemistry* **1997,** *36,* 1018–1025. (c) Rostom, A. A.; Tame, J. R. H.; Ladbury, J. E.; Robinson, C. V. Specificity and Interactions of the Protein Oppa: Partitioning Solvent Binding Effects Using Mass Spectrometry. *J. Mol. Biol.* **2000,** *296,* 269–279. (d) Eckart, K.; Spiess, J. Electrospray Ionization Mass Spectrometry of Biotin Binding to Streptavidin. *J. Am. Soc. Mass Spectrom.* **1995,** *6,* 912–919. (e) Gabelica, V.; de Pauw, E. Comparison between Solution and Gas Phase Kinetic Stability of Oligodeoxynucleotide Duplexes. *J. Mass Spectrom.* **2001,** *36,* 397–402.
4. Butcher, D. J.; Asano, K. G.; Goeringer, D. E.; McLuckey, S. A. Thermal Dissociation of Gaseous Bradykinin Ions. *J. Phys. Chem* **1999,** *103,* 8664–8671.
5. Gao, J.; Wu, Q.; Carbeck, J.; Lei, Q. P.; Smith, R. D.; Whitesides, G. M. Probing the Energetics of Dissociation of Carbonic Anhydrase–Ligand Complexes in the Gas Phase. *Biophys. J.* **1999,** *76,* 3253–3260.
6. (a) Colorado, A; Brodbelt, J. An Empirical Approach to Estimation of Critical Energies by Using a Quadrupole Ion Trap. *J. Am. Soc. Mass Spectrom.* **1996,** *7,* 1116–1125. (b) Apsotol, I. Assessing the Relative Stabilities of Engineered Hemoglobins Using Electrospray Mass Spectrometry. *Anal. Biochem.* **1999,** *272,* 8–18. (c) Wan, K. X.; Gross, M. L.; Shibue, T. Gas Phase Stability of Double-Stranded Oligodeoxynucleotides and Their Noncovalent Complexes with DNA Binding Drugs is Revealed by Collisional Activation in an Ion Trap. *J. Am. Soc. Mass Spectrom.* **2000,** *11,* 450–457. (d) Griffey, R. H.; Sannes-Lowery, K. A.; Drader, J. J.; Mohan, V.; Swayze, E. E.; Hofstadler, S. A. Characterization of Low-Affinity Complexes between RNA and Small Molecules Using Electrospray Ionization Mass Spectrometry. *J. Am. Chem. Soc.* **2000,** *122,* 9933–9938.
7. (a) Poitier, N.; Bart, P.; Tritsch, D.; Biellmann, J. F.; Van Dorsselaer, A. Study of Non-Covalent Enzyme Inhibitor Complexes of Aldose Reductase by Electrospray Mass Spectrometry. *Eur. J. Biochem.* **1997,** *243,* 274–282. (b) Chen, Y.-L.; Campbell, J. M.; Collings, B. A.; Konermann, L.; Douglas, D. J. Stability of a Highly Charged Noncovalent Complex in the Gas Phase: Holomyoglobin. *Rapid Commun. Mass Spectrom.* **1998,** *12,* 1003–1010. (c) Jorgensen, T. J. D.; Delforge, D.; Remacle, J.; Bojensen, G.; Roepstorff, P. Collision-Induced Dissociation of Noncovalent Complexes between Vancomycin Antibiotics and Peptide Ligand Isostereomers: Evidence for Molecular Recognition in the Gas Phase. *Int. J. Mass Spectrom.* **1999,** *188,* 63–85.
8. (a) Laskin, J.; Futrell, J. Internal Energy Distributions Resulting from Sustained Off-Resonance Excitation in Fourier Transform Ion Cyclotron Resonance Mass Spectrometry. II: Fragmentation of the Bromonapthalene Radical Cation. *J. Phys. Chem. A* **2000,** *104,* 5484–5494. (b) Fujiwara, M.; Yasuhide, N. Simulation for Internal Energy Deposition in Sustained Off-Resonance Irradiation Collisional Activation Using a Monte Carlo Method. *Rapid Commun. Mass Spectrom.* **1999,** *13,* 1633–1638.
9. (a) Douglas, D. J.; French, J. B. Collisional Focusing Effects in Radio Frequency Quadrupoles. *J. Am. Soc. Mass Spectrom.* **1992,** *3,* 398–408. (b) Covey, T.; Douglas, D. J. Collision Cross Sections for Protein Ions. *J. Am. Soc. Mass Spectrom.* **1993,** *4,* 616–623.
10. Mauk, A. G.; Mauk, M. R.; Moore, G. R.; Northrup, S. H. Experimental and Theoretical Analysis of the Interaction Be-

tween Cytochrome *c* and Cytochrome b_5. *J. Bioenerg. Biomemb.* **1995,** *27,* 311–329.
11. Northrup, S. H.; Thomassen, K. A.; Miller, C. M.; Barker, P. D.; Eltis, E. D.; Guillemette, J. G.; Inglis, S.; Mauk, A. G. Effects of Charged Amino Acid Mutations in the Bimolecular Kinetics of Reduction of Yeast Iso-1-Ferricytochrome *c* by Bovine Ferrocytochrome b_5. *Biochemistry* **1993,** *32,* 6613–6623.
12. Salemme, F. R. An Hypothetical Structure for an Intermolecular Electron transfer Complex of Cytochrome *c* and b_5. *J. Mol. Biol.* **1976,** *102,* 563–568.
13. Guillimette, J. G.; Barker, P. D.; Eltis, L. D.; Lo, T. P.; Smith, M.; Brayer, G. D.; Mauk, A. G. Analysis of the Bimolecular Reduction of Ferricytochrome *c* by Ferrocytochrome b_5 through Mutagenesis and Molecular Modeling. *Biochimie* **1994,** *76,* 592–604.
14. Mauk, M. R.; Reid, L. S.; Mauk, A. G. Spectrophotometric Analysis of the Interaction between Cytochrome b_5 and Cytochrome *c*. *Biochemistry* **1982,** *21,* 1843–1846.
15. Marzluff, E. M.; Beauchamp, J. L. In *Large Ions: Their Vaporization, Detection and Structural Analysis;* Baer, T.; Ng, C. Y.; Powis, I., Eds.; John Wiley and Sons: New York, 1996; pp 123–129.
16. Chen, Y.-L.; Collings, B. A.; Douglas, D. J. Collision Cross Sections of Myoglobin and Cytochrome *c* ions with Ne, Ar, and Kr. *J. Am. Soc. Mass Spectrom.* **1997,** *8,* 681–687.
17. (a) Marzluff, E. M.; Campbell, S. A.; Rodgers, M. T.; Beauchamp, J. L. Collisional Activation of Large Molecules is an Efficient Process. *J. Am. Chem. Soc.* **1994,** *116,* 6947–6948. (b) Marzluff, E. M.; Campbell, S.; Rodgers, M. T.; Beauchamp, J. L. Low-Energy Dissociation Pathways of Small Deprotonated Peptides in the Gas Phase. *J. Am. Chem. Soc.* **1994,** *116,* 7787–7796.
18. (a) Meroueh, M.; Hase, W. L. Collisional Activation of Small Peptides. *J. Phys. Chem. A* **1999,** *103,* 3981–3990. (b) Meroueh, M.; Hase, W. L. Energy Transfer Pathways in the Collisional Activation of Peptides. *Int. J. Mass Spectrom.* **2000,** *201,* 233–244.
19. Chen, G.; Cooks, R. G.; Bunk, D. M.; Welch, M. J.; Christie, J. R. Partitioning of Kinetic Energy to Internal Energy in the Low Energy Collision-Induced Dissociations of Proton-Bound Dimers of Polypeptides. *Int. J. Mass Spectrom.* **1999,** *187,* 75–90.
20. Nesati, V. unpublished.
21. (a) Ferrer, J. C.; Guillemette, J. G.; Bogumil, R.; Inglis, S. C.; Smith, M.; Mauk, A. G. Identification of Lys 79 as an Iron Ligand in One Form of Alkaline Yeast Iso-1-Ferricytochrome *c*. *J. Am. Chem. Soc.* **1993,** *115,* 7507–7508. (b) Rafferty, S. P.; Pearce, L. L.; Barker, P. D.; Guillemette, J. G.; Kay, C. M.; Smith, M.; Mauk, A. G. Electrochemical, Kinetic, and Circular Dichroic Consequences of Mutations at Position 82 of Yeast Iso-1-Cytochrome *c*. *Biochemistry* **1990,** *29,* 9365–9369. (c) Pollock, W. B. R.; Rosell, F. I.; Twitchett, M. B.; Dumont, M. E.; Mauk, A. G. Bacterial Expression of Mitochondrial Cytochrome. I: Trimethylation of Lys72 in Yeast Iso-1-Cytochrome *c* and the Alkaline Transition. *Biochemistry* **1998,** *3,* 6124–6131.
22. Van Berkel, G.; Zhou, F.; Aronson, J. T. Changes in Bulk Solution pH Caused by the Inherent Current-Controlled Electrolyte Process of an Electrospray Ion Source. *Int. J. Mass Spectrom. Ion Processes* **1997,** *162,* 55–67.
23. Chernushevich, I. V.; Krutchinsky, A. N.; Ens, W.; Standing, K. G. *Proceedings of the 44th ASMS Conference on Mass Spectrometry and Allied Topics*; Portland, OR, 1996; p 751. (b) Schwartz, B. L.; Bruce, J. E.; Anderson, G. A.; Hofstadler, S. A.; Rockwood, A. L.; Smith, R. D.; Chilkoti, A.; Stayton, P. S. Dissociation of Tetrameric Ions of Noncovalent Streptavidin Complexes Formed by Electrospray Ionization. *J. Am. Soc. Mass Spectrom.* **1995,** *6,* 459–465.
24. (a) Hoagland-Hyzer, C. S.; Counterman, A. E.; Clemmer, D. E. Anhydrous Protein Ions. *Chem. Rev.* **1999,** *99,* 3037–3080. (b) Collings, B. A.; Douglas, D. J. Conformation of Gas Phase Myoglobin Ions. *J. Am. Chem. Soc.* **1996,** *118,* 4488–4489.
25. Kraunsoe, J. A. E.; Aplin, R. T.; Green, B.; Lowe, G. An Investigation of the Binding of Protein Proteinase Inhibitors to Trypsin by Electrospray Ionization Mass Spectrometry. *FEBS Lett.* **1996,** *396,* 108–112.
26. Verluis, C.; van der Staaij, A.; Syokvis, E.; Heck, A. J. R.; de Craeme, B. Metastable Ion Formation and Disparate Charge Separation in the Gas Phase Dissection of Protein Assemblies Studied by Orthogonal Time-of-Flight Mass Spectrometry. *J. Am. Soc. Mass Spectrom.* **2001,** *12,* 32–36.
27. Schneider, B. B.; Chen, D. D. Y. Collision Induced Dissociation of Ions Within the Orifice Skimmer-Region of an Electrospray Mass Spectrometer. *Anal. Chem.* **2000,** *72,* 791–799.
28. Millet, F.; Durham, B. Chemical Modifications of Surface residues on Cytochrome *c*. *In Cytochrome c—A Multidisciplinary Approach;* Scott, R. A.; Mauk, A. G., Eds.; University Science Books: Sausalito, CA, 1996; pp 573–591.
29. Rosell, F. I.; Ferrer, J. C.; Mauk, A. G. Proton Linked Protein Conformational Switching: Definition of the Alkaline Conformational Transition of Yeast Iso-1-Cytochrome *c*. *J. Am. Chem. Soc.* **1998,** *120,* 11234–11245.
30. Mauk, A. G.; Mauk, M. R. unpublished.
31. Moore, G. R.; Cox, M. C.; Crowe, D.; Osborne, M. J.; Rosell, F. I.; Bujoms, J.; Barker, P. D.; Mauk, M. R.; Mauk, A. G. N^{ε}, N^{ε}-Dimethyl-Lysine Cytochrome *c* as an NMR Probe for Lysine Involvement in Protein–Protein Complex Formation. *Biochem. J.* **1998,** *332,* 439–449.